ENERGIES AND ELECTRIC DIPOLE MOMENTS OF THE BOUND VIBRATIONAL STATES OF HN_2^+ AND DN_2^+

Vladimír Špirko[a,b1], Ota Bludský[b2] and Wolfgang P. Kraemer[c,*]

[a] *Department of Applied Mathematics and Department of Chemistry, University of Waterloo, Ontario N2L 3G1, Canada*

[b] *Center for Biomolecules and Complex Molecular Systems, Institute of Organic Chemistry and Biochemistry, v.v.i, Academy of Sciences of the Czech Republic, Flemingovo nám. 2, 166 10 Prague 6, Czech Republic; e-mail: [1] vladimir.spirko@marge.uochb.cas.cz, [2] ota.bludsky@marge.uochb.cas.cz*

[c] *Max Planck Institute of Astrophysics, Postfach 1317, D-85741 Garching, Germany; e-mail: wpk@mpa-garching.mpg.de*

Received March 25, 2008
Accepted June 27, 2008
Published online September 17, 2008

Dedicated to Professor Rudolf Zahradník on the occasion of his 80th birthday.

The adiabatic three-dimensional potential energy surface and the corresponding dipole moment surface describing the ground electronic state of HN_2^+ ($\tilde{X}^1\Sigma^+$) are calculated at different levels of *ab initio* theory. The calculations cover the entire bound part of the potential up to its lowest dissociation channel including the isomerization barrier. Energies of all bound vibrational and low-lying ro-vibrational levels are determined in a fully variational procedure using the Suttcliffe–Tennyson Hamiltonian for triatomic molecules. They are in close agreement with the available experimental numbers. From the dipole moment function effective dipoles and transition moments are obtained for all the calculated vibrational and ro-vibrational states. Statistical tools such as the density of states or the nearest-neighbor level spacing distribution (NNSD) are applied to describe and analyse general patterns and characteristics of the energy and dipole results calculated for the massively large number of states of the strongly bound HN_2^+ ion and its deuterated isotopomer.

Keywords: Potential energy and electric dipole hypersurfaces; *Ab initio* CCSD(T) calculations; Effective dipoles and transition moments; Density of states and nearest-neighbor level spacing distributions; Astrochemistry; Interstellar ions.

Protonated N_2, like the isoelectronic isomer pair HCO^+ and HOC^+, have altogether gained great interest in astrophysics and chemistry over the past decades. After the early detection of the famous *U*89 line in dense interstellar clouds[1] and its initial tentative theoretical[2,3] and following experimental identification[4] as $J = 1–0$ rotational transition line of HCO^+, speculations

doi:10.1135/cccc20080873

have soon been made about the possibilities of an interstellar appearance of its isoelectronic analogue, the HN_2^+ ion. First observations of an appropriate triplet of lines toward several warm clouds[5–7] were subsequently verified in the laboratory to be due to protonated nitrogen[8]. Since then much experimental and theoretical effort has been put into more detailed characterizations of this ion; and the lower part of the vibration-rotational spectrum of HN_2^+ is nowadays experimentally well documented[9–20].

On the theory side, apart from an early attempt to predict basic spectroscopic constants of the ion and its isotopomers applying a conventional perturbation approach[21], a more reliable study based on a rather accurate but restricted two-dimensional potential energy surface confirmed for the linear ground electronic state of HN_2^+ equilibrium bond lengths in close agreement with the experimentally determined values and stretching frequencies together with IR intensities[22]. Based on a new fully three-dimensional potential surface calculation on the CCSD(T) level of theory[23], a most comprehensive theoretical coverage of the spectroscopic properties of the HN_2^+ ion was achieved[24]. The vibration-rotational level structure was investigated for all bound states reaching up to the first dissociation threshold and the total number of bound vibrational states ($J = 0$) was found to be as large as about 5000.

In view of the problems arising from handling such a massively large number of bound states for a strongly bound molecular system such as the HN_2^+ ion, it is the intention of the present study to investigate the usefulness of appropriate statistical representations of all bound states and their properties. For this purpose and in order to have a reliable basis for this study, three-dimensional potential energy and electric dipole moment surfaces had to be determined at a high accuracy level of *ab initio* theory.

The high quality of the potential surface calculated for this study is manifested by the fact that the energies obtained for the lower vibration-rotational energy levels and the corresponding rotational and centrifugal distortion constants of the HN_2^+ and DN_2^+ isotopomers are found here to be in excellent agreement with their experimental analogues. On this basis a meaningful discussion of the general patterns of all the bound energy levels and their dipole properties can be started. The main goal of the study is then to check whether standard statistical tools[25–31] for analysing vibrational spectra could be of some help in describing molecular reorganizations which are opposed by surmountable isomerization barriers. The isomerization motion in the HN_2^+ and DN_2^+ isotopomers (migration of the hydrogen atoms around the N_2 core) is opposed by a relatively high barrier (ca. 17 000–18 000 cm^{-1}) which is still much lower than the lowest molecu-

lar dissociation limit: HN_2^+ ($\tilde{X}^1\Sigma^+$) → $H^+ + N_2$ ($\tilde{X}^1\Sigma_g^+$), about 44 000 cm^{-1} above the potential minimum. The pattern of the vibrational energy levels pertaining to the isomerization motion has been found to consist of three qualitatively different substructures (see Fig. 4 of ref.[24]): The "outer" substructures corresponding to the states lying either fairly below or above the barrier consist of reasonably equidistant levels, whereas the "inner" structure is formed by irregularly separated levels. The wavefunctions of the latter states exhibit sizable delocalizations and are thus crucially important for the tunelling isomerization processes. An investigation of the effects of these irregularities in the vibrational level structures on the statistical properties of the two isotopomers appears therefore to be worth a detailed study.

POTENTIAL ENERGY AND ELECTRIC DIPOLE SURFACES

Jacobi coordinates were used for the potential energy and the dipole moment surface determination and in the nuclear dynamics calculations. The NN distance is denoted in this coordinate system by **r** (the norm of the vector **r** joining the two N centers), $R = |\mathbf{R}|$ represents the distance between the center of mass of the NN subunit and H (vector **R** pointing from the center of mass of NN towards H), and θ is the angle between the two vectors **r** and **R**.

The *ab initio* calculations of the potential energy surface were arranged to cover the entire bound part of the potential. The calculations were done at 11 different NN distances in the range $1.60a_0 \le r(\mathrm{NN}) \le 3.00a_0$ and for each *r* value one-dimensional dissociation potentials were determined at 7 different θ angles equally distributed between 0 and 90° with 34 different distances *R* for each angle spanning the wide range $0.7a_0 \le R \le 1000a_0$. According to this scheme energies at more than 2500 individual geometry points were determined to obtain a detailed characterization of the ground state potential surface. C_s point group symmetry was used to classify the electronic wavefunctions. The calculations were done making use of the MOLCAS program system[32].

General contraction type atomic natural orbital (ANO) bases were chosen to approximate the molecular orbitals. They consist of 14s-, 9p-, 4d-, and 3f-type functions contracted to (7s7p4d3f)-functions centered on the nitrogens and for the hydrogen of 8s-, 4p-, and 3d-type functions contracted to (6s4p3d)-functions, i.e. a total of 222 primitive functions contracted to 194 functions.

The energies were calculated at three different theory levels: (i) a coupled-cluster level with all single and double excitations and a perturbational estimate of triple excitations based on canonical SCF orbitals as orbital basis (SCF/CCSD(T)), (ii) the multireference configuration interaction level with all single and double excitations using the CASSCF optimized wavefunction as reference function (CASSCF/MR-CISD), and (iii) applying the second-order Møller–Plesset perturbational approach with CASSCF orbitals as orbital basis (CASPT2). On all these theory levels the two 1s orbitals of the nitrogens were kept frozen and the correlation energy contributions were determined from the remaining valence electrons. In the CASSCF calculations the valence electrons were distributed among 10 active orbitals (8 a′ and 2 a″ orbitals).

Initial test calculations of some basic spectroscopic constants of N_2 and its ion N_2^+ in their ground electronic states ($\tilde{X}\,^1\Sigma_g^+$ and $\tilde{X}\,^2\Sigma_g^+$, respectively) were performed to judge the accuracy of the theory level at which the potential surface calculations of HN_2^+ were done. It turns out that for the diatomic species experimental spectroscopic constants such as equilibrium distances r_e, harmonic frequencies ω_e, or rotational constants B_e were reproduced on the different theory levels equally well within about a 0.1% error limit, whereas for energy values such as the dissociation energies D_0, or the ionization potentials $IP_e(N_2)$ and $IP(N)$ slightly larger average errors of the order of 1%.

For each set of energy data calculated at the three different theory levels, the bound part of the potential including the lowest dissociation channel was obtained by fitting the functional form

$$V(r,R,\theta) = V_0 + \left(\sum_{k,l,m} C(k,l,m)\{\exp[-a_r(r-r_r)]\}^k \times \right.$$

$$\left. \times \{\exp[-a_R(R-R_r)]\}^l \times P_m(\cos\theta) \right) + C_3 R^{-3} + C_4 R^{-4}. \qquad (1)$$

In this expression V_0, $C(k,l,m)$, C_3, C_4, a_r, a_R, r_r, R_r are free parameters and $P_m(\cos\theta)$ are Legendre polynomials. The last two terms were added to improve the flexibility of the function in the range of the potential where the dissociation coordinate R becomes large. Since the coefficients C_3 and C_4 are optimized in the fitting procedure correcting the improper shape of the exponential representation in the large-R region, they are not optimal suitable to provide an exact physically correct asymptotic behavior of the

potential. For the purpose of the present study, however, focussing essentially on the bound ro-vibrational states below and just above the isomerization barrier, the potential representation obtained from Eq. (*1*) is perfectly adequate.

The fits were done in two steps: initially the nonlinear parameters a_r, a_R, r_r, R_r were optimized to achieve optimum flexibility of the fitting function, and then after fixing them at their optimized values, the $C(k,l,m)$ parameters were determined by linear fits. V_0 is the absolute energy minimum of the *ab initio* calculated potential surface and is quoted as theoretical dissociation energy D_e in the following discussion. For the CCSD(T) and MR-CISD theory levels fits were obtained with small standard deviations. Actually, energy points with energies smaller than the isomerization barrier are reproduced by the fits with deviations smaller than about 10 cm^{-1}, whereas for points with energies in the higher region approaching the dissociation limit their representations have larger deviations (between 10 and 100 cm^{-1}). The accuracy of the fitted functions is thus essentially within the accuracy limits of the initial *ab initio* potential energy determinations. The potential function obtained from the CCSD(T) fit was finally used for the following dynamics calculations and the corresponding parameter values are listed in Table I.

The equilibrium bond distances for the linear ground state of NH_2^+ obtained from the potential fits for the different theory levels differ from each other by less than 0.005 Å and are in very close agreement with the corresponding experimental numbers[8] and with the results of the most comprehensive theoretical study on the HN_2^+ ion[24]: r_e = 1.094 Å compared to 1.0928 Å[8] and 1.096 Å[24], and R(H–N) = 1.031 Å compared to 1.0336 Å[8] and 1.034 Å[24]. At dissociation the optimized bond distance of the isolated N_2 was calculated here as 1.096 Å which is again close to the value of 1.0977 Å derived from experiment. For the theoretical dissociation energy D_e the CCSD(T) value with 43 195 cm^{-1} is in reasonable agreement with the 43 243 cm^{-1} obtained in ref.[24], whereas the energies obtained at the other theory levels (about 43 610 cm^{-1}) are noticeably larger. The geometry parameters for the transition state at the isomerization barrier ($\theta = \pi/2$) were calculated as r(NN) = 1.124 Å (1.126 Å[24]) and R(H–NN) = 1.151 Å (1.155 Å[24]). For the height of the isomerization barrier there is again a difference between the CCSD(T) result with 17 055 versus 17 613 cm^{-1} on the other two levels (ref.[24] reports 17 134 cm^{-1}).

The in-plane electric dipole moment components were evaluated relative to the molecular center of mass directly as expectation values from the iterated MR-CISD wavefunctions for all the different molecular geometries

incorporated in the potential energy determination. For fitting the dipole moment component functions, the ion is defined to be oriented in the body-fixed coordinate system such that it is placed in the (*y*,*z*)-plane with the *z*-axis embedded along the **R** vector and with the origin of the coordinate system at the center of mass. In this reference configuration the μ_y component turns out to be rather small and it changes only little over the entire surface. It was therefore assumed to be equal to zero in the present calculations. The μ_z component of the dipole moment, asymptotically linear in *R*, was expressed as

$$\mu_z(r,R,\theta) = \frac{m_H}{m_H + 2m_N} R + \left(\sum_{k,l,m} D(k,l,m) \times r\{\exp[-a_r r]\}^k \times \right.$$

$$\left. \times \; R\{\exp[-a_R R]\}^l \times P_m(\cos\theta) \right) + D_0 R + D_1 R^{-1} + D_2 R^{-2} + D_3 R^{-3} \qquad (2)$$

where $D(k,l,m)$, D_0, D_1, D_2, D_3 are adjustable parameters, P_m are Legendre polynomials, and m_H, m_N are the atomic masses. The parameters a_r and a_R were kept fixed after a preliminary fitting. The standard deviation of this dipole fit is 0.20 D. Table II shows the fitted parameters obtained for the dipole moment function.

NUCLEAR DYNAMICS CALCULATIONS

The rotation-vibrational energy levels of the ground electronic state of HN_2^+ and DN_2^+ were determined using the Sutcliffe–Tennyson Hamiltonian[33], expressed in the following form after integration over angular coordinates[34]

$$\mathbf{H}^{ST} \equiv ||\langle jk|\mathcal{H}_j^{ST}(r,R,\theta)|j'k'\rangle|| -$$

$$- \hbar^2 \delta_{j,j'} \delta_{k,k'} \times \left(\frac{1}{2\mu_1} \frac{\partial^2}{\partial r^2} + \frac{1}{2\mu_2} \frac{\partial^2}{\partial R^2} - \right.$$

$$\left. - j(j+1) \left\{ \frac{1}{2\mu_1 r^2} + \frac{1}{2\mu_2 R^2} \right\} - \frac{J(J+1) - 2k^2}{2\mu_2 R^2} \right) -$$

$$- \delta_{j,j'} \frac{\hbar^2}{2\mu_2 R^2} \times \left(C^+_{J,k} C^+_{j,k} \delta_{k,k+1} + C^-_{J,k} C^-_{j,k} \delta_{k,k+1} \right) +$$

$$+ \delta_{k,k'} \sum_{\lambda} g_\lambda (j,j',k)\, V_\lambda (r,R) \qquad (3)$$

with $C^{\pm}_{l,k} = [l(l+1) - k(k \pm 1)]^{1/2}$ and where μ_1 and μ_2 are the appropriate reduced masses, j is the bending vibrational quantum number, (J,k) are the

TABLE I

Potential energy function parameters (in cm^{-1}) for the ground electronic state of HN_2^+ obtained by fitting the expression of Eq. (*1*) to the *ab initio* energy points calculated at the CCSD(T) level[a]

k	*l*	*m*	*C*(*k*,*l*,*m*)	*k*	*l*	*m*	*C*(*k*,*l*,*m*)	*k*	*l*	*m*	*C*(*k*,*l*,*m*)	*k*	*l*	*m*	*C*(*k*,*l*,*m*)
1	0	0	104011.195	1	2	1	–223197.906	2	3	2	148514.875	0	6	0	–1694.603
0	1	0	–62615.066	0	3	1	152875.969	1	4	2	–138705.500	1	2	0	–44437.203
2	0	0	–258623.719	3	1	1	89405.055	0	5	2	25822.838	0	3	0	37196.078
2	1	0	209277.984	2	2	1	434397.344	3	3	2	–62013.535	2	2	0	124103.477
1	2	0	–229311.406	1	3	1	–266257.000	2	4	2	51650.637	1	3	0	–104939.133
0	3	0	103931.578	0	4	1	–7817.504	0	6	2	–4114.040	0	4	0	3374.140
3	1	0	–226522.812	3	2	1	–339528.625	0	1	3	–29112.996	3	2	0	–109324.688
2	2	0	183403.406	2	3	1	257038.969	1	1	3	94727.711	2	3	0	86493.953
1	3	0	7629.381	1	4	1	–71000.922	2	1	3	–103701.156	4	2	0	31763.074
0	4	0	–68619.711	0	5	1	31151.980	1	2	3	10310.791	3	3	0	–23579.975
5	0	0	82914.781	4	2	1	75998.570	0	3	3	21382.879	1	5	0	–590.580
4	1	0	77538.422	3	3	1	–54812.137	3	1	3	38216.645	0	1	0	892.952
3	2	0	–55849.172	2	4	1	8107.494	2	2	3	–14433.102	1	1	0	–2760.112
1	4	0	–12386.323	1	5	1	3213.171	1	3	3	–97167.336	0	2	0	1121.592
0	5	0	29259.846	0	6	1	–5411.249	0	4	3	28141.242	2	1	0	1621.112
2	4	0	3138.542	1	2	2	–20537.146	2	3	3	142138.047	1	2	0	–861.689
0	6	0	–4916.937	0	3	2	27862.506	1	4	3	–73914.062	1	1	0	464.938
0	1	1	–89857.227	1	3	2	–64825.086	0	5	3	10031.315	0	2	1	–363.191
1	1	1	219594.781	0	4	2	36165.129	3	3	3	–52088.738	2	1	1	–439.736
2	1	1	–231505.109	4	1	2	1164.599	2	4	3	27761.021	1	2	1	352.075

[a] C_3 = –59219.755 cm^{-1}, C_4 = 207614.111 cm^{-1}; the nonlinear parameters a_r = 1.0 $Å^{-1}$, a_R = 1.19 $Å^{-1}$; r_r = 1.094869 Å, R_r = 1.578718 Å held fixed after their preliminary determination.

rotational quantum numbers, and $g_\lambda(j,j',k)$ are the Gaunt coefficients[35]. $V_\lambda(r,R)$ represents the potential of Eq. (*1*) after performing the Sutcliffe–Tennyson integration

$$V(r,R,\theta) = \sum_\lambda V_\lambda(r,R)\, P_\lambda(\cos\theta)\,. \qquad (4)$$

The variational solution of the eigenvalue problem was achieved by diagonalizing the above Hamiltonian matrix (Eq. (*3*)) in terms of basis sets which, apart from Legendre polynomials for the bending functions, consisted of eigenfunctions obtained numerically from the corresponding uncoupled one-dimensional Schrödinger equations for the stretching motions along the *r* and *R* coordinates. Numerical basis functions are known to be superior compared with analytical functions such as for example harmonic oscillator functions which are often used in algebraic solutions of vibrational eigenvalue problems. In order to be able to describe all the bound states up to the highly excited levels close to the dissociation threshold with sufficient accuracy, large and flexible basis sets were employed consisting of 30 numerical functions for the high-frequency NN-stretching coordinate *r*, 55 numerical functions for the low-frequency stretching coordinate *R*, and 60 bending basis functions. The actual basis contained 11 311 product functions for HN_2^+ and 12 244 functions for DN_2^+. It is stressed here again that even much larger basis sets would be required when aiming of the same accuracy level if the numerical stretching functions were replaced by analytical functions.

TABLE II
Electric dipole moment function parameters (in D) for the ground electronic state of HN_2^+ obtained by fitting the expression of Eq. (*2*) to the *ab initio* dipole moment data obtained from the MR-CISD wavefunctions[a]

k l m	*D*(*k*, *l*, *m*)	*k l m*	*D*(*k*, *l*, *m*)	*k l m*	*D*(*k*, *l*, *m*)	*k l m*	*D*(*k*, *l*, *m*)	*k l m*	*D*(*k*, *l*, *m*)
1 0 0	4.5275	3 0 0	3.7054	3 2 0	–1.3541	0 2 2	19.1966	1 3 2	–3.9033
0 1 0	1.6585	0 3 0	–44.8154	0 5 0	–4.9055	2 1 2	–4.5848	0 4 2	6.8703
2 0 0	–8.0303	1 3 0	2.0846	0 1 2	–6.9761	0 3 2	–19.0531	1 1 4	–0.2162
0 2 0	22.1101	0 4 0	26.2060	1 1 2	3.9693	2 2 2	4.4611	0 2 4	0.7437
0 3 4	–0.3607								

[a] D_0 = 4.6012 D, D_1 = –10.2954 D Å, D_2 = 6.4966 D Å^2, D_3 = –1.1276 D Å^3; the nonlinear parameters a_r = 0.02 Å^{-1}, a_R = 0.220316 Å^{-1} held fixed after their preliminary determination.

STATISTICAL ANALYSIS

Standard statistical approaches described in the literature[25–31] were applied to characterize the properties of some of the calculated quantities. The nearest-neighbur spacing distribution (NNSD) is one of the simplest quantities in this context used for the local analysis when fitted to the Brody distribution[36]

$$P_{\mathrm{Bro}} = (\omega + 1)\alpha s^{\omega} \exp(-\alpha s^{\omega+1}) \tag{5}$$

with $\alpha = [\Gamma((\omega + 2)/(\omega + 1))]^{\omega+1}$ and where the phenomenological Brody parameter ω is used to semi-quantitatively describe the degree of the chaos in the quantum dynamical system. For the two extreme cases, $\omega = 1$ and 0, the Brody distribution coincides, respectively, with the Wigner distribution[37]

$$P_{\mathrm{Wig}} = \frac{\pi}{2} s \exp\left(-\frac{\pi}{4} s^2\right) \tag{6}$$

TABLE III
Experimental and calculated energies (in cm^{-1}) of the lowest vibrational and $J = l_2$ rotational levels of HN_2^+ and DN_2^+

v_1	$v_2^{l_2}$	v_3	Exp.[a]	Calc.	Exp.	Calc.
			HN_2^+		DN_2^+	
0	$1^{\pm1}$	0	688.373	687.515	544.468[b]	543.904
0	2^{0}	0	1363.337	1364.843		1081.247
0	$2^{\pm2}$	0	1386.503	1385.236		1093.197
0	$3^{\pm1}$	0	2051.359	2053.533		1630.702
0	$3^{\pm3}$	0	2093.978	2092.620		1647.536
0	0^{0}	1	2257.873	2247.073	2024.041[c]	2018.082
0	4^{0}	0	2726.230	2728.692		2161.390
0	$4^{\pm2}$	0	2748.833	2750.336		2173.968
0	$4^{\pm4}$	0	2810.354	2809.217		2206.623
0	$1^{\pm1}$	1	2946.617	2936.619		2564.420
1	0^{0}	0	3233.958	3233.604	2636.982[d]	2631.048
1	$1^{\pm1}$	0	3898.680	3899.231	3163.242[d]	3157.072

[a] Ref.[19], [b] ref.[13], [c] ref.[10], [d] ref.[11]

predicted by the random matrix theory which corresponds to a completely chaotic case, and the Poisson distribution[38]

$$P_{\mathrm{Pois}} = \exp(-s) \tag{7}$$

corresponding to fully integrable dynamics. In all these expressions

TABLE IV
Experimental and calculated rotational constants B_v (in cm^{-1}) and centrifugal distortion constants D_v (in 10^{-6} cm^{-1}) of the lowest vibrational and $J = l_2$ rotational levels of HN_2^+ and DN_2^+

v_1	l_2 v_2	v_3	B_{exp} [a]	D_{exp} [a]	B_{cal} [b]	D_{cal} [b]	B_{cal} [c]	D_{cal} [c]	B_{exp} [d]	D_{exp} [d]	B_{cal} [c]	D_{cal} [c]
					HN_2^+						DN_2^+	
0	0^0	0	1.55392	2.89	1.547	2.9	1.55093	2.94	1.28605[d]	2.05	1.28422	2.06
0	1^{+1}	0	1.55326	3.16	1.547	2.9	1.55014	2.96	1.28693[d]	2.08	1.28511	2.09
0	1^{-1}	0	1.56173	3.29	1.555	3.0	1.55860	3.06	1.29423[d]	2.18	1.29239	2.18
0	2^0	0	1.56160	9.29	1.555	8.6	1.55834	9.71			1.29346	14.45
0	2^{-2}	0	1.56093	5.77	1.554	3.0	1.55737	3.06			1.29307	2.20
0	2^{+2}	0	1.56049	–3.68	1.554	–2.6	1.55736	–3.55			1.29308	–9.97
0	3^{+1}	0	1.55638	4.97	1.550	5.1	1.55325	5.34			1.29064	6.89
0	3^{-1}	0	1.57386	5.78	1.567	5.3	1.57057	5.80			1.30550	7.63
0	3^{+3}	0	1.56312	0.91	1.556		1.55992	0.83			1.29718	–1.69
0	3^{-3}	0	1.56316	1.67	1.556		1.55992	0.73			1.29711	–3.00
0	0^0	1	1.54291	2.63	1.537	2.3	1.53969	2.95	1.27809[d]	2.05	1.27616	2.06
0	4^0	0	1.56943	23.2	1.563	20.4	1.56609	22.3			1.30280	35.8
0	4^{-2}	0	1.56859	7.03	1.561	5.0	1.56507	5.27			1.30245	6.26
0	4^{+2}	0	1.56837	–13.7	1.562	–12.1	1.56503	–13.9			1.30246	–27.1
0	4^{+4}	0	1.56516	1.05			1.56202	1.05			1.30102	–1.62
0	4^{-4}	0	1.56516	1.05			1.56202	1.10			1.30102	–1.62
0	1^{+1}	1	1.54185	1.74	1.536	2.9	1.53835	2.92			1.27636	2.13
0	1^{-1}	1	1.55061	3.13	1.544	3.0	1.54723	3.07			1.28420	2.17
1	0^0	0	1.54132	2.87	1.535	2.9	1.53835	2.92	1.27450[d]	2.01	1.27252	2.01
1	0^{+1}	0	1.54087	3.07	1.534	2.8	1.53780	2.92	1.27683[e]	1.86	1.27475	1.97
1	0^{-1}	0	1.54948	3.18	1.543	3.0	1.54638	3.04	1.28314[e]	1.86	1.28127	2.11

[a] Ref.[19], [b] ref.[24], [c] present calculation, [d] ref.[20], [e] ref.[11]

$$s = \frac{S}{D} = \frac{\text{spacing}}{\text{mean spacing}} \qquad (8)$$

where spacing means in the present context the difference between energies or effective dipoles of adjacent levels of the same symmetry and mean spacing is its averaged value.

The shapes of the standard distribution functions are derived under a set of simplifying assumptions. In general they provide only a qualitative description of the numerically derived distributions. However, in order to get

TABLE V
Coefficients (in cm^{-1}) of the vibrational energy term formula of Eq. (*11*) for the low lying vibrational states of HN_2^+ and DN_2^+ [a]

k	*l*	*m*	*C*(*k*,*l*,*m*)	*k*	*l*	*m*	*C*(*k*,*l*,*m*)	*k*	*l*	*m*	*C*(*k*,*l*,*m*)
							HN_2^+				
1	0	0	3403.394	2	1	0	0.2521454	2	0	2	0.2263882
0	1	0	1386.604	2	0	1	–3.7328790	1	3	0	–0.0324283
0	0	1	2286.019	1	2	0	–0.1946181	1	2	1	–0.1640400
2	0	0	–69.82826	1	1	1	1.9409890	0	4	0	–1.0838620
1	1	0	–46.30142	0	3	0	1.1794510	0	1	3	–0.0247541
1	0	1	–15.26862	0	2	1	0.2077752	5	0	0	0.0016694
0	1	1	–8.484573	0	0	3	0.2387719	0	5	0	0.2480011
0	0	2	–13.50880					0	6	0	–0.0288773
								0	7	0	0.0016968
								0	8	0	–0.0000400
							DN_2^+				
1	0	0	2719.033	3	0	0	0.6887511	4	0	0	–0.0360610
0	1	0	1091.172	2	1	0	0.5737271	1	3	0	0.0360213
0	0	1	2060.912	2	0	1	0.4850224	1	2	1	–0.1181748
2	0	0	–23.61578	1	2	0	0.2228044	0	4	0	–0.1636878
1	1	0	–37.93500	1	0	2	–1.14037330	0	1	3	–0.1065540
1	0	1	–49.08952	0	2	1	–1.1933630	0	5	0	0.0219050
0	2	0	3.486832	0	1	2	0.4987691	0	0	5	–0.0010354
0	1	1	6.411305					0	6	0	–0.0007839
0	0	2	–10.48017								

[a] 110 lowest states of HN_2^+ with $v_2 \leq 10$ and 130 lowest states of DN_2^+ with $v_2 \leq 11$ reproduced with ~1 cm^{-1} standard devitations.

a more quantitative representation of these distributions a number of empirical functions were probed. In the present case the following two empirical expressions were found to give accurate fits to the numerical distribution results

$$P_{\mathrm{edf1}} = C_1 P_{\mathrm{Wig}}(s) + C_2 s \exp[-C_3(s - C_4)] \qquad (9)$$

and

$$P_{\mathrm{edf2}} = C_1 s^3 \exp[-C_3(s - C_2) - C_4(s - C_2)^3] \qquad (10)$$

TABLE VI
Coefficients (in D) of the electric dipole term formula[a] for the low-lying vibrational states of HN_2^+ and DN_2^+

k	l	m	$\mathcal{D}(k,l,m)$	k	l	m	$\mathcal{D}(k,l,m)$	k	l	m	$\mathcal{D}(k,l,m)$
							HN_2^+				
0	0	0	3.48968	2	1	0	0.00431	2	0	2	0.00260
1	0	0	0.08627	1	1	1	0.00144	1	3	0	0.00013
0	1	0	–0.10645	0	2	1	0.00115	0	4	0	–0.00001
0	0	1	–0.03790	0	1	2	0.00253				
2	0	0	0.01344	0	0	3	–0.00078				
1	1	0	–0.01529								
1	0	1	0.03660								
0	2	0	0.00231								
0	1	1	–0.01377								
							DN_2^+				
0	0	0	3.50705	3	0	0	–0.00139	2	0	2	0.00180
1	0	0	–0.01546	2	1	0	–0.00113	0	4	0	–0.00002
0	1	0	–0.05188	2	0	1	–0.00913				
0	0	1	–0.00797	1	1	1	–0.00173				
1	1	0	0.00508	1	0	2	–0.00779				
1	0	1	0.04429	0	3	0	0.00064				
0	2	0	–0.00313	0	0	3	–0.00018				
0	1	1	0.00228								

[a] $\mu(v_1,v_2,v_3) = \sum_{k,l,m} \mathcal{D}(k,l,m)(v_1 + \frac{1}{2})^k (v_2 + \frac{1}{2})^l (v_3 + \frac{1}{2})^m$; 110 lowest states of HN_2^+ with $v_2 \leq 10$ and 130 lowest states of DN_2^+ with $v_2 \leq 11$ reproduced with ~0.01 D standard devitations.

(C_i (i = 1, 4) being "free" parameters) for the energy and effective dipoles, respectively. The function of Eq. (*9*), an extension of the Wigner distribution function (*6*), has previously been found to give a quantitatively accurate representation of the numerical energy level distributions in the case of the FHF^- negative ion[30].

RESULTS AND DISCUSSION

The lowest vibrational states of the HN_2^+ and DN_2^+ ions show a level structure which corresponds to systems with strongly linear geometries. For the assignment of these lower levels it is thus suitable to make use of the quantum numbers that are commonly used to describe the dynamics of linear molecules. For some of the higher states, however, which exhibit a noticeable tunnelling behavior ("tunnelling" states), this labeling system becomes inappropriate and quantum numbers characterizing nonlinear molecule motions[39] are required instead. The quantum numbers actually applied in the present study were thus v_1 to account for the H–N and v_3 for the N–N stretching vibrations and $v_2^{l_2}$ and v_2 to label the low-lying and "tunnelling" bending states, respectively.

The excellent agreement of the present calculated lowest vibrational levels with their experimental analogues is illustrated in Table III. The energies

TABLE VII
Typical vibrational transition moments $|\langle v_1'' v_2'' v_3'' | \mu_z | v_1' v_2' v_3' \rangle|$ (in D) for the low-lying vibrational states of HN_2^+

000←000	3.446[a]	100←100	3.589	010←010	3.347	001←001	3.463
200←200	3.716	020←020	3.238	030←030	3.137	002←002	3.458
000←100	0.244[b]	100←200	0.357	200←300	0.452	300←400	0.537
010←110	0.244	110←210	0.357	210←310	0.453	310←410	0.538
001←101	0.244	101←201	0.358	201←301	0.452	301←401	0.536
000←010	0.050	010←020	0.096	020←030	0.139	030←040	0.178
100←110	0.052	110←120	0.099	120←130	0.140	130←140	0.177
001←011	0.050	011←021	0.095	021←031	0.137	031←041	0.175
000←001	0.014	001←002	0.017	002←003	0.019	003←004	0.018
010←011	0.008	011←012	0.010	012←013	0.010	013←014	0.009
100←101	0.034	101←102	0.046	102←103	0.053	103←104	0.057

[a] Experimental value[18]: 3.4 (±0.2) D, [b] experimental value[17]: 0.23 (±0.02) D.

are given relative to the zero-point energies obtained here at 3496.9 cm^{-1} for HN_2^+ and at 2911.0 cm^{-1} for DN_2^+ (for comparison, in ref.[24] for HN_2^+ a value of 3507.8 cm^{-1} has been given). The agreement between calculations and experiment is mostly within a few wavenumber units; mainly levels involving the N–N stretching excitations show deviations up to about 10 cm^{-1}. Similarly, the present calculated rotational constants B_v and centrifugal distortion constants D_v of the lowest vibrational states are also very close to the corresponding constants derived from experiments (Table IV). The close matching of the low-lying vibration-rotational levels shown in the two tables evidences thus the high accuracy of the calculations and of the theory applied here and it demonstrates its adequacy to make physically correct predictions of the studied states. All the calculated states lying below the isomerization barrier (treating the tri-atomic ion as nonlinear species there are 165 states for HN_2^+ and 265 states for its deuterated isomer, in the linear case there would be much more which are in the present treatment considered as rotational states) can be assigned safely and their energies are fitted fairly quantitatively (Table V) using the standard Dunham expansion

$$G(v_1,v_2,v_3) = \sum_{k,l,m} C(k,l,m)\left(v_1+\frac{1}{2}\right)^k\left(v_2+\frac{1}{2}\right)^l\left(v_3+\frac{1}{2}\right)^m . \qquad (11)$$

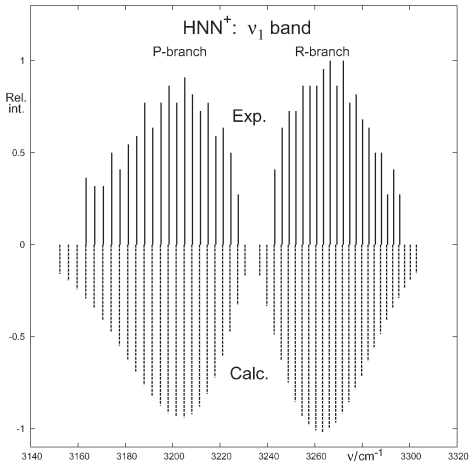

FIG. 1
Calculated and experimental (ref.[40]) ν_1 absorption band of HN_2^+

This holds also for the effective dipole moments $\langle v_1 v_2 v_3 | \mu_z | v_1 v_2 v_3 \rangle$ (Table VI). These calculated moments exhibit a higher degree of mode specificity than the corresponding energies and they allow therefore a safer assignment of the calculated states. The fitted expressions actually do not only reproduce closely the energies and moments of the fitted lowest states, but they also provide quite accurate predictions for the stretching states lying quite above the isomerization barrier. The calculated data are in excellent agreement with the corresponding available experimental numbers as documented in Table VII and in Fig. 1. The quasi-linearity of the HN_2^+ ion is underlined by the fact that for the lower vibrational states in Table III the energy difference between the $l_2 = 0$ and $\Delta l_2 = \pm 2$ levels is initially small,

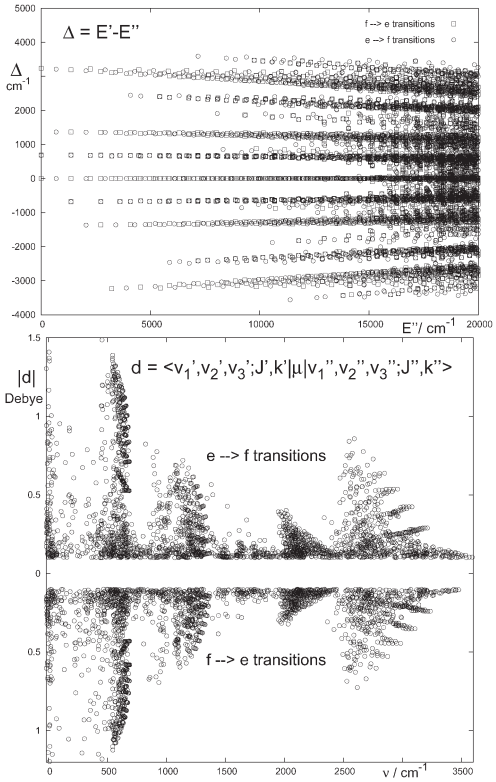

FIG. 2
Calculated values of the $\Delta k = 1$ (e $\rightarrow f$ and $f \rightarrow$ e) frequencies (upper panel) and transition moments (lower panel) for $J = 1$, $k = 0$ and 1 states of HN_2^+

increasing, however, for higher vibrational states as illustrated also in the upper panel of Fig. 2 which shows that the patterns of the f → e and e → f transition plots are increasingly non-parallel with increasing excitation energy and become finally rather chaotic in the energy region close to the isomerization barrier. This figure demonstrates that the mode specificity of the states lying below the isomerization barrier also holds for the rota-

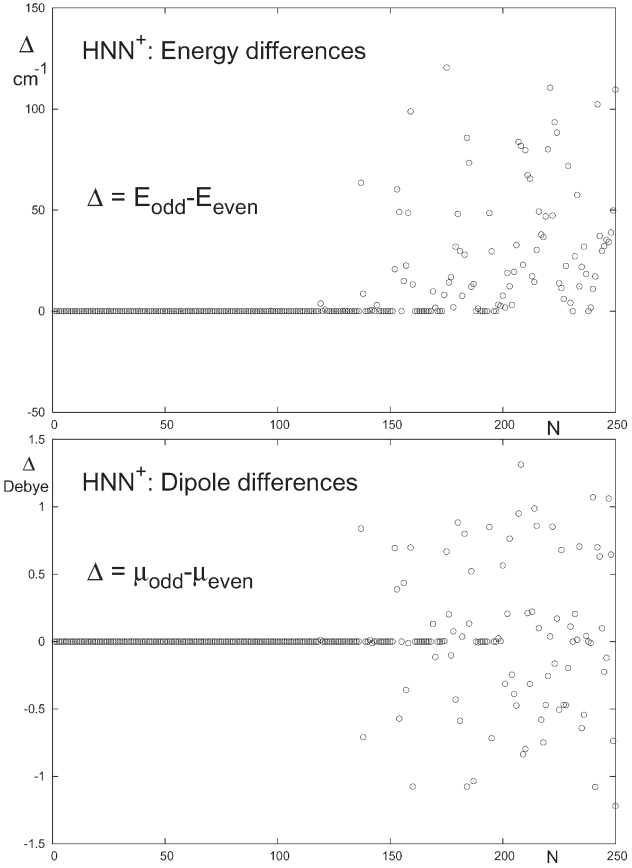

FIG. 3

Differences between the energies (upper panel) and electric dipoles $\langle v_1 v_2 v_3 | \mu_z | v_1 v_2 v_3 \rangle$ (lower panel) of the antisymmetric (odd) and symmetric (even) vibrational states of HN_2^+. The states are labeled by the integer N increasing according to the energy content of the states

tional states allowing thus a better rationalization of the observed spectral patterns.

The Dunham expansion, however, becomes inappropriate when trying to represent states with higher excitations of the bending mode (v_2). Whereas expression (*11*) is still perfectly adequate for reproducing the quasi-degenerate states with bending energy contents smaller than the

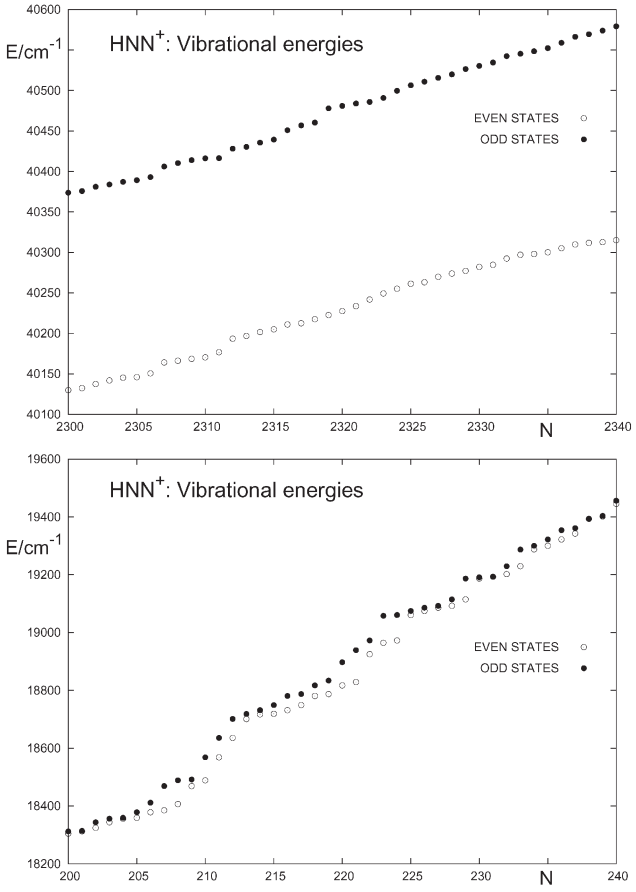

FIG. 4
Calculated values of the vibrational energies of states lying energetically either only slightly above (lower panel) or much above (upper panel) the isomerization barrier. Labeling of states as in Fig. 3

isomerization barrier, it fails to describe levels with bending energies comparable to the barrier energy. These states exhibit irregular tunnelling splittings as shown in Fig. 3 and can obviously not be fitted by any simple energy formula. States, on the other hand, with bending energy contents

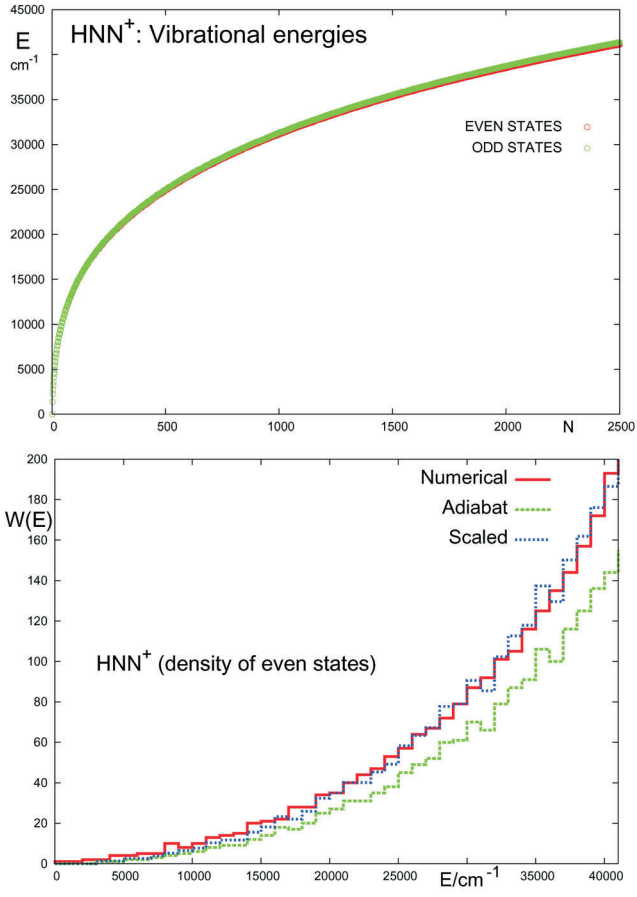

FIG. 5

Calculated values of the bound even and odd vibrational states of HN_2^+ (upper panel) and the cumulative spectral density function of the even states (lower panel). $W(E)$ counts the number of states containing energies up to E. "Numerical" represents the numerically exact results, "Adiabat" the results obtained using the adiabatic approximation, and "Scaled" marks the plot obtained by scaling the adiabatic results by a factor of 1.295. Labeling of states as in Fig. 3

much higher than the isomerization barrier assume a free-rotor pattern and could, at least in principle, be fitted by an appropriate energy term formula. An actual attempt, however, to obtain a fit of these and other highly excited states becomes soon impractical because the intrinsic complexity of the energy pattern and the density of states grow rapidly with increasing

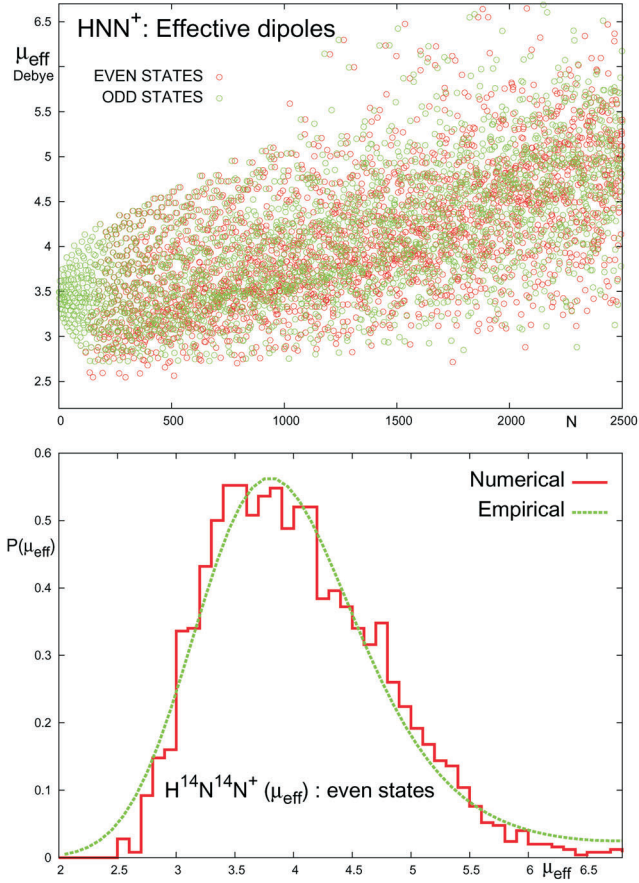

FIG. 6

Calculated effective electric dipoles of the bound states of HN_2^+ (upper panel) and a histogram of their magnitudes (lower panel), where "Numerical" represents the numerically exact results, whereas "Empirical" labels results obtained by smoothing the calculated data using the empirical expression of Eq. (*10*). Labeling of states as in Fig. 3

excitation. These highly excited states are strongly mixed and their assignments in terms of distinct quantum numbers are thus meaningless. Other description techniques focussing more on a characterization of the global behavior of the large number of states are required instead. Characterizations of this kind are used in Figs 5–8 to describe the energy and effective dipole moment data of such highly excited states. It should be noted at this point that the characteristics corresponding to the odd symmetry levels exhibit exactly the same shapes as their even symmetry counterparts and that

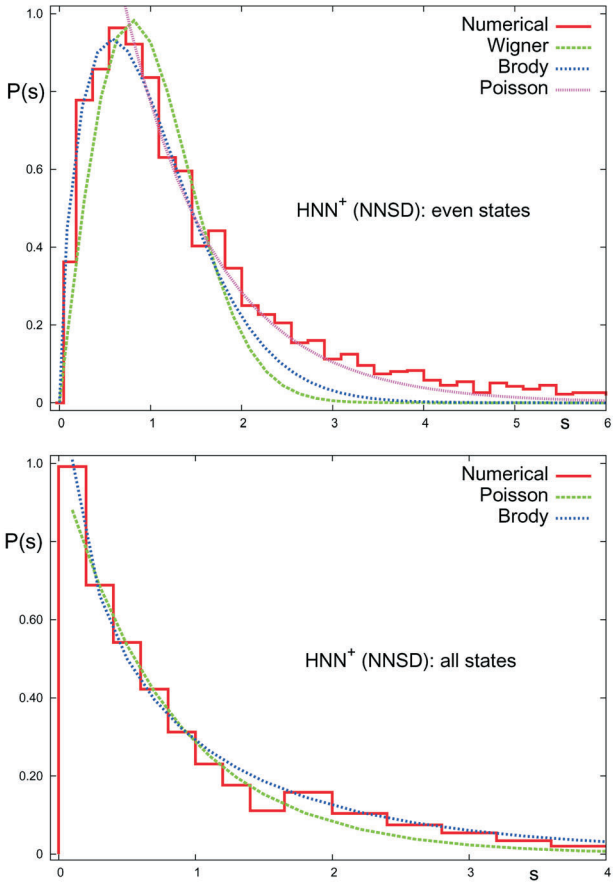

FIG. 7
The nearest-neighbor energy level spacing distributions of the even states (upper panel) and for both symmetry states (lower panel), respectively

the functional forms of the calculated characteristics are practically mass-independent.

From the upper panel of Fig. 5 it follows that the energies of the states lying above the isomerization barrier increase rather slowly and smoothly perturbed by only small-amplitude fluctuations as demonstrated for two different energy regimes in the two panels of Fig. 4. A similar smooth global

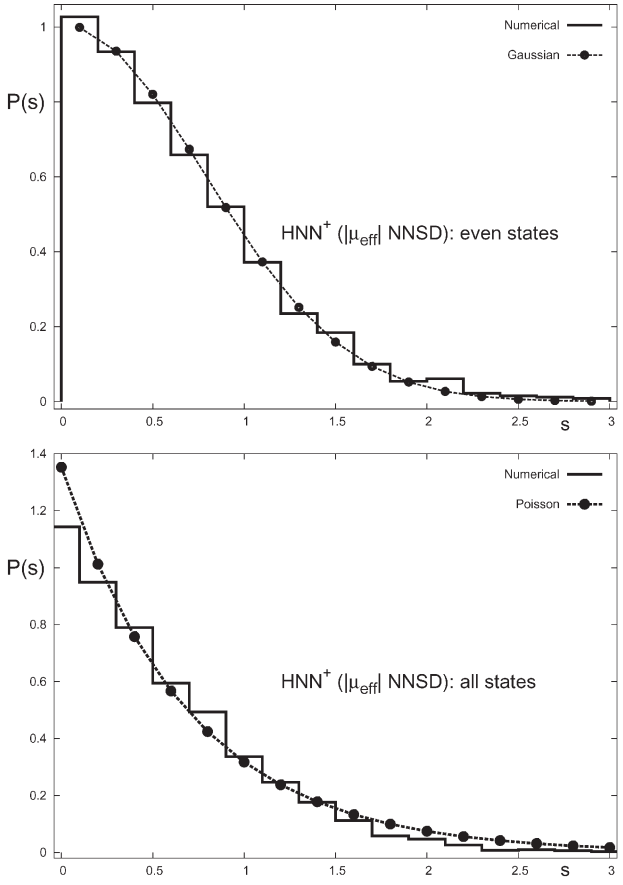

FIG. 8
The nearest-neighbor electric dipole spacing distributions of the even states (upper panel) and for both symmetry states (lower panel), respectively

behavior follows therefore for the level density of states plotted in the lower panel of Fig. 5. A direct evaluation of this level density function $W(E)$, which plays an essential role in the statistical theories of the rate constants, by a straightforward diagonalisation of the dynamical Hamiltonian is, however, unfeasible for large molecular systems. Reliable approximate strategies for its evaluation need to be introduced.

As pointed out earlier in our former study on FHF^- (see Fig. 1 in ref.[30]), a possible way to simplify this problem can be found by applying an appropriate adiabatic separation of the dynamical variables with largely different energy contents. In the present case a corresponding adiabatic approximation can be obtained when averaging over the high-frequency N–N stretch motion and transforming thus the three-dimensional problem into a set of two-dimensional eigenvalue equations for the remaining low-frequency motions, the H···NN stretch and the bending. However, due to larger non-adiabatic couplings in HN_2^+, this separation is not as quantitative as in the previously studied FHF^- negative ion. On the other hand, the plots in the lower panel of Fig. 5 show that the exact numerical level density and its adiabatic approximation are essentially in good agreement with each other differing only by a constant scaling factor. In contrast to the smooth energy curves in this figure, the corresponding excitation dependence of the effective electric dipoles appears to be rather chaotic as illustrated in the upper panel of Fig. 6. The lower panel shows, on the other hand, that its statistical distribution function $P(\mu_{\mathrm{eff}})$ can be represented rather accurately in terms of the fairly simple Maxwellian curve obtained when fitting the empirical expression of Eq. (*10*).

The statistical behavior of the nearest-neighbor spacing distributions (NNSD) of the calculated vibrational energies and effective electric dipole moments are displayed in Figs 7 and 8. As in all other systems studied in the literature (cf., e.g., refs[29,30] and references therein), the distribution of the nearest-neighbor energy spacings of correlated ("single symmetry") energy levels has a maximum at a finite value (even states in the upper panel of Fig. 7), whereas the corresponding distribution of the nearest-neighbor effective dipole spacings coincides practically with a Gaussian-like distribution (upper panel of Fig. 8) as can be expected from ref.[40]. The energy distribution of the even states in the peak region is best represented by a Brody distribution, while in the tail region for larger s values the distribution resumes the Poisson character. The distributions obtained for all states of both symmetries (lower panels of the two figures) resemble the Poisson distribution throughout. An expected striking indication for a tunnelling ef-

fect in the energy distributions does not seem to be evidenced by the present calculations.

However, it is interesting to refer at this point to the results obtained previously for a model system[41] which describes the tunnelling motion of a particle confined in a *x*,*y*-rectangular infinite well with a very thin but high wall centered at $x = y$. In this system the antisymmetric states comply with the Poissonian behavior, but the symmetric (tunnelling) states give rise to a NNSD with a finite peak in a narrow interval at the smallest energy spacings and only the remaining distribution is again essentially Poissonian (see Fig. 2 of ref.[41]). While in the present calculations no difference is obtained for the distributions of the states of different symmetry, the NNSD of the even states in the upper panel of Fig. 7 does actually show a peak at a small energy spacing and a Poissonian behavior in the tail region. Rather than interpreting this finding as a safe indication for a tunnelling effect, more detailed tests of the impact of tunnelling states on nearest-neighbor level spacing distributions are required.

CONCLUSIONS

Energies and electric dipole transition moments of the ro-vibrational states of strongly bound HNN^+ and DNN^+ cations are evaluated *ab initio* applying a high state-of-the-art level of theory. The low-lying states are fitted, fairly quantitatively, using the Dunham expansions allowing thus for meaningful assignments of these states in terms of the standard vibrational and rotational quantum numbers. The calculated characteristics are found to be in excellent agreement with available experimental data ensuring thus that the results predicted for the so far unobserved states are reliable.

To gain insight into their global behavior, the calculated higher excited states are characterized by their densities and nearest-neighbor level spacing distributions (NNSD). With the exception for the distribution of the nearest-neighbor energy spacings of the correlated (“single symmetry”) energy levels, the calculated characteristics resume shapes which are in reasonable agreement with their theoretical counterparts predicted by the random-matrix theory. The shapes of the “anomalous” single-symmetry energy spacing distributions acquire forms which are close to the distribution function pertaining to the symmetric states of a one-dimensional model consisting of an infinite rectangular well with a δ-function finite barrier. We find it thus legitimate to surmise that this shape could be an indication of the tunnelling motion. To get a convincing support for this conjecture, we plan more detailed calculations which will probe the energy

spacing distributions as functions of the barrier widths and heights varying over a wide-range of their values.

This work was a part of the research project Z40550506 and was supported by the Grant Agency of the Academy of Sciences of the Czech Republic (Grant No. A400550511) and by the Ministry of Education, Youth and Sports of the Czech Republic (Grant No. LC512). The work was initiated when V. Špirko was visiting the University of Waterloo and was completed when W. P. Kraemer was visiting the Center for Biomolecules and Complex Molecular Systems. Financial support and hospitality of the hosting institutes are gratefully acknowledged.

REFERENCES

1. Buhl D., Snyder L. E.: *Nature* **1970**, *228*, 267.
2. Wahlgren U., Liu B., Pearson P. K., Schaefer H. F.: *Nature* **1973**, *246*, 4.
3. Kraemer W. P., Diercksen G. H. F.: *Astrophys. J. Lett.* **1976**, *205*, L97.
4. Woods R. C., Dixon T. A., Saykally R. J., Szanto P. G.: *Phys. Rev. Lett.* **1975**, *35*, 1269.
5. Turner B. E.: *Astrophys. J. Lett.* **1974**, *193*, L83.
6. Green S., Montgomery J. A., Jr., Thaddeus P.: *Astrophys. J. Lett.* **1974**, *193*, L89.
7. Thaddeus P., Turner B. E.: *Astrophys. J. Lett.* **1975**, *201*, L25.
8. Saykally R. J., Dixon T. A., Anderson T. G., Szanto P. G., Woods R. C.: *Astrophys. J. Lett.* **1976**, *205*, L101.
9. Gudeman C. S., Begemann M. H., Pfaff J., Saykally R. J.: *J. Chem. Phys.* **1983**, *78*, 5837.
10. Foster S. C., McKellarA. R. W.: *J. Chem. Phys.* **1984**, *81*, 3424.
11. Nesbitt D. J., Petek H., Gudeman C. S., Moore C. B., Saykally R. J.: *J. Chem. Phys.* **1984**, *81*, 5281.
12. Sears T. J.: *J. Opt. Soc. Am. B* **1985**, *2*, 786.
13. Sears T. J.: *J. Chem. Phys.* **1985**, *82*, 5757.
14. Owrutsky J. C., Gudeman C. S., Martner C. C., Tack L. M., Rosenbaum N. H., Saykally R. J.: *J. Phys. Chem.* **1986**, *84*, 605.
15. Owrutsky J. C., Keim E. R., Coe J. V., Saykally R. J.: *J. Phys. Chem.* **1989**, *93*, 5960.
16. Sasada H., Amano T.: *J. Chem. Phys.* **1990**, *92*, 2248.
17. Keim E. R., Polak M. L., Owrutsky J. C., Coe J. V., Saykally R. J.: *J. Chem. Phys.* **1990**, *93*, 3111.
18. Havenith M., Zwart E., Meerts W. L., ter Meulen J. J.: *J. Chem. Phys.* **1990**, *93*, 8446.
19. Kabbadj Y., Huet T. R., Rehfuss B. D., Gabrys C. M., Oka T.: *J. Mol. Spetrosc.* **1994**, *163*, 180.
20. Amano T., Hirao T., Takano J.: *J. Mol. Spetrosc.* **2005**, *234*, 170.
21. Hennig P., Kraemer W. P., Diercksen G. H. F.: *MPI/PAE Astro-Report*. Max Planck Institute of Physics and Astrophysics, Munich 1977.
22. Botschwina P.: *Chem. Phys. Lett.* **1984**, *107*, 535.
23. Schmatz S.: *Globale Potentialhyperflächen und genaue Schwingungszustandsdichten am Beispiel der Kationen NH_2^+ und HCO^+*. Cuvillier Verlag, Göttingen 1986.
24. Schmatz S., Mladenović M.: *Ber. Bunsenges. Phys. Chem.* **1997**, *101*, 372.
25. Wigner E. P.: *Proc. Cambridge Philos. Soc.* **1951**, *47*, 790.
26. Porter C. E.: *Statistical Theories of Spectra: Fluctuations*. Academic Press, New York 1965.

27. Mehta M. L.: *Random Matrices and the Statistical Theory of Energy Levels, Random Matrices*. Academic Press, New York 1967.
28. Percival I. C.: *J. Phys. B* **1973**, *6*, L229.
29. Guhr T., Müller-Groeling A., Weidenmüller H. A.: *Phys. Rep.* **1998**, *299*, 189.
30. Špirko V., Šindelka M., Shirsat R. N., Leszczynski J.: *Chem. Phys. Lett.* **2003**, *376*, 595.
31. Peroncelli L., Grossi G., Aquilanti V.: *Mol. Phys.* **2004**, *102*, 2345.
32. Andersson K., Blomberg M. R. A., Fülscher M. P., Karlström G., Lindh R., Malmqvist P.-A., Neogrády P., Olsen J., Roos B. O., Sadlej A. J., Schütz M., Seijo L., Serrano-Andrés L., Siegbahn P. E. M., Widmark O.-O.: *MOLCAS*, Version 5. Lund University, Lund 2002.
33. Sutcliffe B. T., Tennyson J.: *Mol. Phys.* **1986**, *58*, 1053.
34. Tennyson J., Miller S., LeSueur C. R.: *Comp. Phys. Commun.* **1993**, *75*, 339.
35. Buehler R. O., Hirschfelder J. O.: *Phys. Rev.* **1951**, *83*, 628.
36. Brody T. A., Flores J., French J. B., Mello P. A., Pandey A., Wong S. S. M.: *Rev. Mod. Phys.* **1981**, *53*, 385.
37. Wigner E. P.: *Phys. Rev.* **1932**, *40*, 749.
38. Berry M. V., Tabor M.: *Proc. R. Soc. London, Ser. A* **1977**, *356*, 374.
39. Boháček I., Papoušek D., Pick Š., Špirko V.: *Chem. Phys. Lett.* **1976**, *42*, 395.
40. Abul-Magd A. Y.: *Phys. Rev. E* **2006**, *73*, 056119.
41. Lewenkopf C. H.: *Phys. Rev. A* **1990**, *42*, 2431.
42. Nakanaga T., Ito F., Sugawara K., Takeo H., Matsumura C.: *Chem. Phys. Lett.* **1990**, *169*, 269.